Inorganic Chemistry

Article

pubs.acs.org/IC

Probing Hydrogen Bond Networks in Half-Sandwich Ru(II) Building Blocks by a Combined ^{1}H DQ CRAMPS Solid-State NMR, XRPD, and DFT Approach

Michele R. Chierotti, Roberto Gobetto,* and Carlo Nervi

Department of Chemistry and NIS Centre of Excellence, University of Torino, Via P. Giuria 7, 10125 Torino, Italy

Alessia Bacchi and Paolo Pelagatti

Department of Chemistry, University of Parma, Parco Area Scienze 17/A, 43124 Parma, Italy

Valentina Colombo and Angelo Sironi*

Department of Chemistry, University of Milano, Via Golgi 19, 20133 Milano, Italy

Supporting Information

ABSTRACT: The hydrogen bond network of three polymorphs (**1α**, **1β**, and **1γ**) and one solvate form (**1·H$_2$O**) arising from the hydration−dehydration process of the Ru(II) complex [(*p*-cymene)Ru(κN-INA)Cl$_2$] (where INA is isonicotinic acid), has been ascertained by means of one-dimensional (1D) and two-dimensional (2D) double quantum ^{1}H CRAMPS (Combined Rotation and Multiple Pulses Sequences) and ^{13}C CPMAS solid-state NMR experiments. The resolution improvement provided by homonuclear decoupling pulse sequences, with respect to fast MAS experiments, has been highlighted. The solid-state structure of **1γ** has been fully characterized by combining X-ray powder diffraction (XRPD), solid-state NMR, and periodic plane-wave first-principles calculations. None of the forms show the expected supramolecular cyclic dimerization of the carboxylic functions of INA, because of the presence of Cl atoms as strong hydrogen bond (HB) acceptors. The hydration−dehydration process of the complex has been discussed in terms of structure and HB rearrangements.

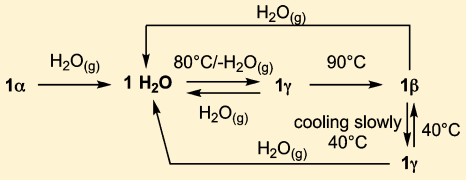

INTRODUCTION

Noncovalent interactions are key features in determining crystal packing differences and, thus, property differences in polymorphic and solvate systems.[1] Among all weak interactions, the hydrogen bond (HB) is the most important because it combines directionality and strength with selectivity, leading to one-dimensional (1D), two-dimensional (2D), or three-dimensional (3D) architectures, or new co-crystals with peculiar properties.[2]

The characterization of different HB-based polymorphs represents an important challenge, since it implies the study of weak interactions, which are responsible for the unique properties shown by each polymorph. This allows packing-property correlations to be made and then the design of periodic and organized structures with desired and tunable features. In these studies, X-ray single-crystal diffraction (XRSCD) is certainly the best technique, which is, nevertheless, not suitable when dealing with very small crystals (powders). In the latter case, a reliable alternative is ab initio powder X-ray diffraction (XRPD),[3] which can be profitably complemented by solid-state NMR (SSNMR) and density functional theory (DFT) computational methods.[4] Indeed, XRPD provides long-range information such as (time and space) averaged symmetry and atomic positions, while SSNMR relies on local (short-range) information at each independent site to address the "size" of the asymmetric unit and the stereochemistry of relevant fragments and tectons (by looking at ^{1}H−^{1}H and ^{1}H−^{13}C proximities).[5] Very fast magic angle spinning (MAS) at 70 kHz or Combined Rotation and Multiple Pulses Sequences (CRAMPS) such as DUMBO, PMLG, ..., etc.[6] allow the location of hydrogen-bonded proton signals, which experience high-frequency shifts, the magnitudes of which are strongly dependent on HB length and strength.[7] On the other hand, by means of ^{1}H 2D double-quantum (DQ) MAS or CRAMPS NMR experiments, it is possible to obtain additional information on intramolecular and intermolecular ^{1}H−^{1}H proximities up to ∼3.0 Å, which is useful for elucidating HB networks. DFT-based periodic calculations applied to the solid state help to solve structures, elucidate spectroscopic properties, and determine energy differences between polymorphs, or even prevent incorrect structure determination from powder data.[8]

Received: July 10, 2013
Published: December 16, 2013

We have recently characterized the behavior of a promising building block for wheel-and-axle systems: the half sandwich Ru(II)-complex [(*p*-cymene)Ru(κN-INA)Cl_2] (**1**, where INA is isonicotinic acid).[9] Wheel-and-axle (WAA) compounds are dumbbell-shaped molecules where a linear ditopic ligand bridges two relatively bulky groups.[10] These systems are able to reversibly absorb several volatile organic compounds through heterogeneous solid−gas processes,[11] thus being good candidates for the development of gas sensors or gas-storage devices. In our case, INA was expected to bind Ru through the py-N donor and, at the same time, give rise to the cyclic dimerization of the COOH functions, thus creating the axle of the WAA system. Although the py-binding to Ru was confirmed, the COOH groups dimerization was prevented by the formation of intermolecular Ru−Cl···HOOC HBs isolating the room-temperature stable polymorph **1*α*** (see Scheme 1a).

Scheme 1. (a) General Scheme with Atom Labeling of 1, [(*p*-cymene)Ru(κN-INA)Cl_2], with the Hydrogen Bonding Motif Characterizing 1*α* and 1*β*. (b) Hydrogen Bonding Motif of 1·H_2O. (c) Originally Proposed Hydration−Dehydration Process of Complex 1 (General Scheme with Relevant Atom Labelling and Hydrogen Bonding Motif of 2, [(*p*-cymene)Ru(κN-A4AB)Cl_2])

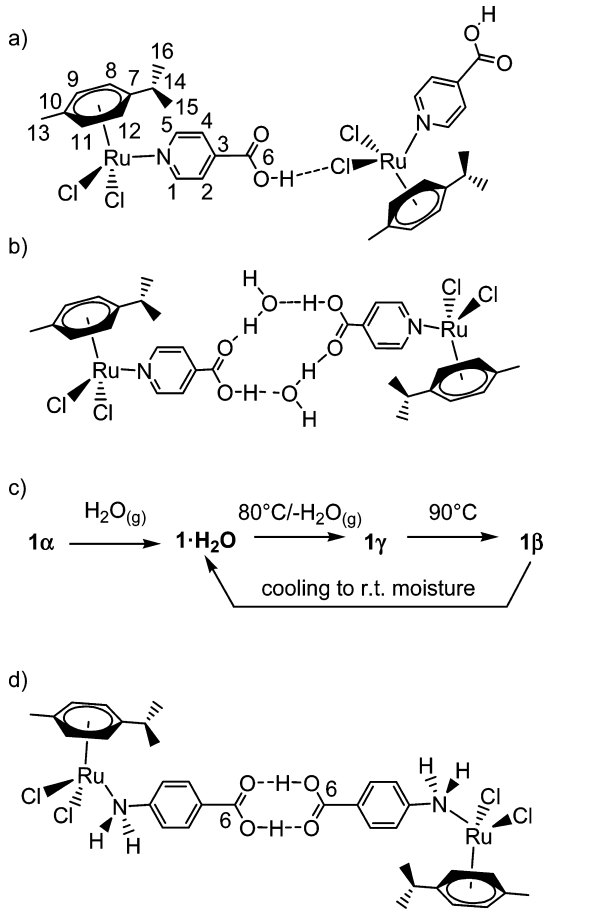

Once exposed to water vapors, **1*α*** quickly converted to **1·H_2O** (Scheme 1b) that, upon heating, afforded an anhydrous polymorph, **1*β*** (Scheme 1a), through a transient intermediate, **1*γ***. Such hydration−dehydration processes are summarized in Scheme 1c. All the reported phases, except **1*γ***, were structurally characterized either by XRSCD (**1*α*** and **1·H_2O**) or the XRPD and SSNMR approach (**1*β***).[9]

The number of studies dealing with organometallic polymorphism is certainly limited if compared to the huge amounts of reports on organic polymorphism,[12] possibly because the main field of application of organometallics (i.e., homogeneous catalysis) concerns their solutions.

Here, we report on the isolation of the pure **1*γ*** polymorph and its XRPD/NMR/DFT structural characterization that was previously hindered by the lack of long-standing pure samples. Thermodiffractometry allowed the recognition of pure **1*γ*** at RT and, later, its structural characterization. The use of ^{1}H MAS and CRAMPS (*w*PMLG5) and ^{1}H 2D DQ CRAMPS (PMLG5-POSTC7-*w*PMLG5) SSNMR techniques has been fundamental for adding spectroscopic evidence on HB networks in all forms. Periodic plane-wave DFT calculations were actively used to confirm and refine all experimental information. Eventually, this synergic coupling of different approaches led to a better understanding of the entire system.

In light of these new results, this paper is also an opportunity to discuss the hydration−dehydration process of the Ru(II) complex in terms of HB, crystal packing rearrangements and polymorph stabilities. For a thorough analysis, forms **1*α*** and **1·H_2O**, whose X-ray structures are available, will be used for comparison together with the analogue Ru(II) complex [(*p*-cymene)Ru(κN-A4AB)Cl_2] (**2**)[13] (where A4AB is 4-aminobenzoic acid) (Scheme 1d) and the free ligands INA and A4AB.

EXPERIMENTAL DETAILS

SSNMR Spectroscopy. SSNMR measurements were made on a Bruker AVANCE II 400 instrument operating at 400.23 and 100.65 MHz for ^{1}H and ^{13}C, respectively. ^{13}C and ^{1}H−^{13}C HETCOR spectra were recorded at RT at the spinning speed of 12 kHz. Cylindrical 4-mm outer diameter (O. D.) zirconia rotors with sample volume of 80 μL were employed. For ^{13}C CPMAS experiments, a ramp cross-polarization pulse sequence was used with contact times of 4 ms, a ^{1}H 90° pulse of 3.30 μs, recycle delays of 1.5 s, and 1024 transients. The two-pulse phase modulation (TPPM) decoupling scheme was used with a frequency field of 75 kHz. 2D ^{1}H−^{13}C on- and off-resonance HETCOR spectra were measured according to the method of van Rossum et al.,[14] using the setup previously described.[15] The ^{1}H chemical shift scale in the HETCOR spectra was corrected by a scaling factor of $3^{-1/2}$, since the ^{1}H chemical shift dispersion is scaled by a factor of $3^{-1/2}$ during FSLG decoupling. ^{1}H MAS, ^{1}H CRAMPS, and 2D ^{1}H DQ CRAMPS experiments were performed on a 2.5-mm Bruker probe. The ^{1}H MAS spectra were acquired at the spinning speed of 32 kHz with the DEPTH sequence ($\pi/2-\pi-\pi$) for the suppression of the probe background signal. ^{1}H CRAMPS spectra were acquired using a windowed-PMLG (*w*PMLG5)[16] pulse sequence of dipolar decoupling at the spinning speed of 12.5 kHz. 2D ^{1}H DQ CRAMPS spectra were acquired at the spinning speed of 12.5 kHz with PMLG5 and *w*PMLG5 pulse sequences for homonuclear dipolar decoupling during t_1 and t_2, respectively. For all samples, ^{1}H 90° pulse lengths of 2.5 μs and recycle delays of 3 s were used. For each of 256 increments of t_1, 80 transients were averaged. The pulse width and the RF power were finely adjusted for best resolution. In t_2, one complex data point was acquired in each acquisition window (2.2 μs). DQ excitation and reconversion was achieved using three elements of POST-C7,[17] corresponding to a recoupling time of 68.58 μs. A 16-step nested phase cycle was used to select $\Delta p = \pm 2$ on the DQ excitation pulses (four steps), and $\Delta p = -1$ on the *z*-filter 90° pulse (four steps). The States-TPPI method was used to achieve sign discrimination in the F1 dimension. ^{1}H and ^{13}C scales were calibrated with adamantane (^{1}H signal at 1.87 ppm) and glycine (^{13}C methylene signal at 43.86 ppm) as external standards.

X-ray Powder Diffraction (XRPD) Measurements and Analysis. All the diffraction data (Cu $K\alpha_{12}$, λ = 1.5418 Å) were

dx.doi.org/10.1021/ic401762z | Inorg. Chem. 2014, 53, 139−146

collected on a θ:θ Bruker AXS D8 AVANCE vertical scan diffractometer; the generator was operated at 40 kV and 40 mA. The diffractometer was equipped with a nickel filter and a linear position-sensitive detector (PSD), with the following optics: primary and secondary Soller slits, 2.3° and 2.5°, respectively; divergence slit, 0.3°; and receiving slit, 8 mm. The nominal resolution for the present setup is 0.08° 2θ (fwhm of the α_1 component) for the LaB_6 peak at ~21.3° (2θ). The conditioning chamber for thermodiffractometric experiment, a closed Peltier sample heater, was supplied by Officina Elettrotecnica di Tenno, Italy. The accurate diffraction pattern at RT under nitrogen of the pure **1γ** phase was acquired in the 4°−90° 2θ range, with $\Delta 2\theta$ = 0.02° and exposure time = 1 s/step. The pattern was indexed using the single value decomposition approach,[18] which afforded a monoclinic lattice ($P21/a$ space group, a = 30.986(2) Å, b = 15.3681(9) Å, c = 7.3828(4) Å, β = 95.281(4)°; Le Bail R_{wp} = 4.39) later confirmed by finding, upon exhaustive simulated annealing runs,[19] a good structural hypothesis (R_{wp} = 10.15), which was successfully refined (final R_p, R_{wp}, and R_{Bragg}: 4.02, 5.28, and 2.27, respectively).

During simulated annealing, we described the molecule as a single "flexible" rigid body allowing for all necessary rotations. At variance, during refinements, the Ru-(η^6-*p*-cimene) and the *p*-carboxyl pyridine groups were treated as independent, "flexible" (both the isopropyl and carboxyl group rotations were allowed), rigid bodies. The Cl atoms were free to refine but the Ru−Cl and Ru−N bond distances were restrained to 2.44 and 2.12 Å, respectively. "Antibump" conditions were substantial for a correct sampling of the conformational space.[20] The final refinement was done using the DFT optimized structure as "reference" (see main text and ref 32), maintaining only the Ru−Cl and Ru−N restraints.

Peak shapes were described by the fundamental parameters approach.[21] The experimental background was fit by a polynomial description. Systematic errors were modeled with sample-displacement angular shifts corrections. To metal and Cl atoms was given a refinable isotropic displacement parameter (BM), while to lighter atoms was assigned a common B = BM + 2.0 Å^2 value. All computations were performed with TOPAS, using scattering factors, corrected for real and imaginary anomalous dispersion terms, taken from its internal library.[22]

Computational Details. Periodic lattice calculations were performed by means of Quantum Espresso, version 4.3.2,[23] keeping the cell parameters (i.e., no cell optimizations have been performed) and the Ru atom coordinates constant, which are the most accurate XRPD parameters. Vanderbilt Ultrasoft pseudo-potentials (USPP),[24] including scalar relativistic corrections, were used for all atoms (employing those available at the Quantum Espresso website).[25] The general gradient approximation (GGA) with the Perdew−Burke−Ernzerhof (PBE) functional[26] was used in the calculations. We thoroughly used a cutoff energy of 60 Ry for plane-wave USPP calculations to ensure convergence. The high cutoff chosen is required by the presence of atoms, like oxygen, for which even the ultrasoft pseudo-potential is relatively hard. Note, however, that a lower level of convergence would not affect the conclusions drawn in this work significantly. Because of the large cell size and their shapes, the irreducible Brillouin zones were sampled with only one (for **1β**) or two *k*-points (2 × 1 × 1 for **1γ**), with the Monkhorst−Pack scheme.[27] The Gaussian 09[28] GIAO method has been used to compute NMR chemical shifts of **1γ**. We employed the DFT method with Becke's three-parameter hybrid functional[29] and Lee−Yang−Parr's gradient-corrected correlation functional (B3LYP).[30] The Los Alamos double-ζ (LanL2Dz) basis set and effective core potential were used for Ru atoms, and the split-valence 6-31+G(d,p) basis set was applied for all other atoms. The chemical shifts were computed by extracting two structures from the optimized **1γ** cell unit: four and three molecules of the first neighboring shell have been selected around the strong and the weak H···Cl interactions, respectively. The calculated absolute magnetic shielding σ values were converted to ^{1}H chemical shifts δ, relative to the absolute magnetic shielding of TMS (σ = 31.6412), computed at the same B3LYP/6-31+G(d,p) level.

RESULTS AND DISCUSSION

Solid-State Synthesis of 1γ and Reformulation of the Qualitative Phase Diagram. VT-XRPD experiments show that, although **1β** can be stabilized at RT by quenching from 90 °C to RT, it is only metastable. Indeed, if slowly cooled, it transforms to **1γ**. The **1β** → **1γ** phase transition occurs at ca. 35 °C, while the backward transformation **1γ** → **1β** starts above 40 °C. The same experiment performed by keeping the temperature constant just above the onset (80 °C), confirm the crystal-to-crystal nature of the **1·H$_2$O** → **1γ** and **1γ** → **1β** transformations (see Figure S1 in the Supporting Information). The instability of **1γ** at 80 °C and the inherent presence of some phase contamination (heavy in the intermediate at 80 °C but only slight at RT), do not hamper confirmation that the powder pattern of the intermediate phase **1γ**, reported in Figure 1c, well matches that obtained by cooling under N_2 (Figure 1e).

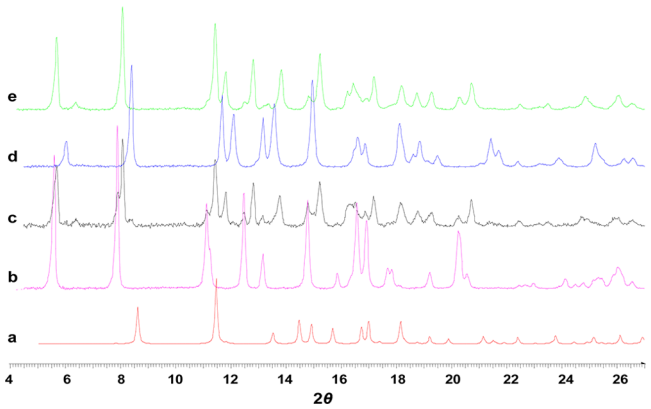

Figure 1. Powder patterns of (a) **1α**, as calculated from the single crystal structure; (b) **1·H$_2$O** at RT; (c) **1γ**, as recorded after 300 min annealing at T = 80 °C of **1·H$_2$O**; (d) **1β** at T = 373 K; (e) **1γ** as recorded after cooling at RT, under N_2 atmosphere, of **1β**.

Thus, the originally proposed qualitative phase diagram (Scheme 1c) must be redrawn as in Scheme 2. The lack of amorphous intermediates during the **1·H$_2$O** → **1γ** and **1γ** → **1β** processes and their reversibility indicate their topotactic nature, i.e., the structures of **1·H$_2$O**, **1γ**, and **1β** must have a high degree of similarity.

Scheme 2. New Hydration−Dehydration Processes of the Complex [(*p*-cymene)Ru(κN-INA)Cl$_2$]

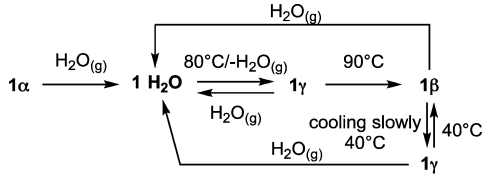

The characterization of the hydration−dehydration processes has been completed by the ab initio XRPD structural determination of **1γ** taking full advantage of the complementary information granted by SSNMR and computational techniques.

SSNMR Data on 1γ. ^{1}H and ^{13}C chemical shifts with assignments for compound **1γ** are reported in Table 1. ^{1}H and ^{13}C assignments have been based on data of **1α** and **1β** previously reported[9] and with the help of the ^{1}H−^{13}C FSLG-HETCOR experiment (see Figure S2 in the Supporting Information). However, it was not possible to discriminate

dx.doi.org/10.1021/ic401762z | Inorg. Chem. 2014, 53, 139−146

Table 1. ^{1}H and ^{13}C Chemical Shifts (ppm) with Assignments for Compound 1γ[a]

carbon[b]	type	^{13}C δ	^{1}H δ C–H
C1	CH	160.3/159.5	9.1 H1
C2	CH	120.8/120.0	7.1 H2
C3	C_q	139.7/137.1	
C4	CH	123.3/122.2	6.6/6.5 H4
C5	CH	153.8/153.3	8.8/8.9 H5
C6	COOH	167.3/162.9	10.5 H10 OH[b]
C7	C_q	100.5/99.9	
C8	CH	79.2	5.0 H8
C9	CH	89.9/87.0	5.5/5.5 H9
C10	C_q	97.4	
C11	CH	86.5sh/84.3	5.6/5.4 H11
C12	CH	83.2/80.5	5.0/5.4 H12
C13	CH_3	19.2/17.3	1.7/1.4 H13
C14	CH	30.8	3.2 H14
C15	CH_3	26.8/24.9	1.8/1.6 H15
C16	CH_3	19.2	1.4 H16

[a]For atom labeling, see Scheme 1a. [b]It was not possible to individuate the other OH signal due to overlap with other resonances. Thus, only the OH involved in the strong O–H···Cl HB is reported.

and assign the resonances (in particular, the ^{1}H resonances are still quite broad) for the symmetry nonequivalent molecules. The splitting of all ^{13}C resonances in the ^{13}C CPMAS spectrum of **1γ**, shown in Figure 2a, which is not observed for **2** (Figure

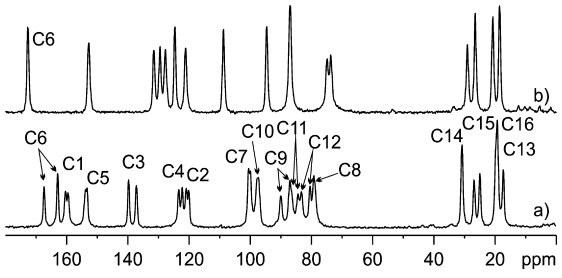

Figure 2. ^{13}C (100.65 MHz) CPMAS spectra with relevant signal assignments of compounds (a) **1γ** and (b) **2** recorded with a spinning speed of 12 kHz.

2b), clearly highlights the presence of two independent molecules in the unit cell (Z' = 2; for a thorough comparison, ^{13}C spectra of **1α**, **1·H$_2$O**, and **1β** are reported in Figure S3 in the Supporting Information). The chemical shift difference (~4.4 ppm) for the two C6 (COOH) nuclei in **1γ** (167.3 and 162.9 ppm) suggests two different HB arrangements. However, both sites do not seem to form the cyclic dimerization, which would result in a high-frequency shift similar to that observed in **2**, (C6 at 172.7 ppm, Figure 2b). The cyclic dimerization is definitely ruled out by the analysis of the DQ correlations in the ^{1}H DQ CRAMPS spectrum, where the presence of DQ signals implies a ^{1}H–^{1}H through-space separation of less than ~3 Å with $\delta_{DQ} = \delta_A + \delta_B$ for $^{1}H^{A}$–$^{1}H^{B}$ proximities (two symmetric signals, with respect to the diagonal) or $\delta_{DQ} = 2\delta_A$ for $^{1}H^{A}$–$^{1}H^{A}$ intermolecular separation (one peak on the diagonal).[31] In the case of compound **2**, whose spectrum is reported in Figure 3, the presence of the COOH cyclic motif (which brings two OH of different molecules closer than 3 Å) leads to a DQ coherence at δ_{DQ} = 13.3 + 13.3 = 26.6 ppm (diagonal correlation), as expected. In contrast, in the ^{1}H DQ CRAMPS spectrum of **1γ**,

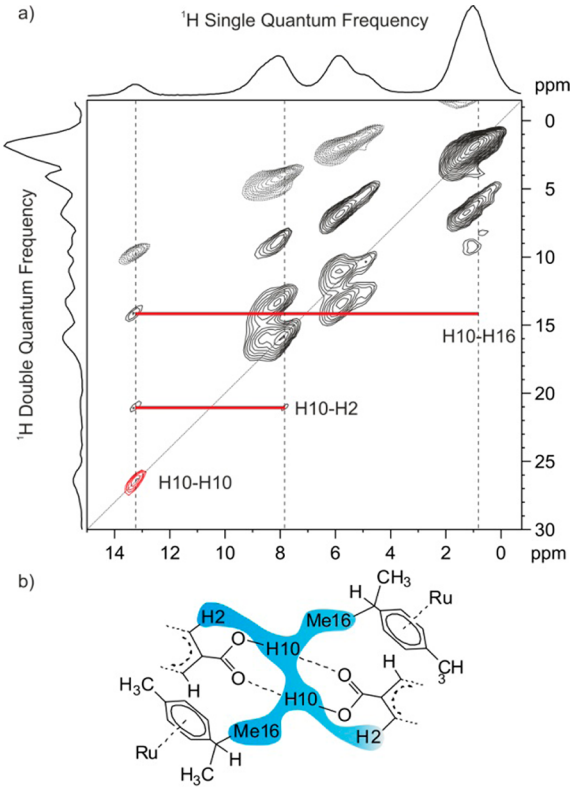

Figure 3. (a) ^{1}H (400.23 MHz) DQ CRAMPS (PMLG5–POSTC7–*w*PMLG5) spectrum of **2**, together with skyline projections recorded at 12.5 kHz MAS. Negative contours (artificial peaks) and the F1 = 2F2 diagonal are shown as dashed lines. Solid red horizontal bars indicate specific DQ coherences between OH (H10) and nearby protons. The OH diagonal peak indicating the cyclic dimerization of the COOH groups is highlighted in red. (b) Representation of the crystal structure of **2** showing the intermolecular proximity between H10 and H16 and the intramolecular proximity between H10 and H2.

shown in Figure 4, the lack of DQ coherences at δ_{DQ} = 10.5 + 10.5 = 21.0 ppm definitively indicates the absence of COOH dimerization. Other DQ signals involving OH protons are collected in Table 2.

The comparison between ^{1}H MAS spectra of **1β** and **1γ**, reported in Figure 5, shows a halving of the **1β** OH signal intensity. This can be attributed either to a reduction of the number of protons involved in the O–H···Cl or to the presence of a very weak HB leading to a OH signal overlapped with that of the aromatic protons. Proton mobility along the HB has been ruled out by recording spectra at different temperatures.

Crystal Structure of 1γ and a Short Reappraisal of That of 1β. The structure of **1γ** was solved, ab initio, from laboratory XRPD patterns. **1γ** crystallizes in the monoclinic, $P2_1/a$, space group (No. 14, nonstandard setting of $P2_1/c$) with two independent molecules in the asymmetric unit (Z = 8, Z' = 2) and the largest molecular volume, $V_M = V/Z$, among the three anhydrous polymorphs **1α**, **1γ**, and **1β** (421, 437, and 425 Å^3, respectively). The molecular structure and labeling scheme of **1γ** are reported in Figure 6.

XRPD, particularly when using laboratory instruments, affords blurry molecular pictures. Presently, dealing with two molecules in the asymmetric unit (with a volume of 874 Å^3) and 44 independent non-hydrogen atoms, we were forced to use a heavy idealization. In the present case, diffraction possibly affords only the rough shape and location of the two

dx.doi.org/10.1021/ic401762z | *Inorg. Chem.* 2014, 53, 139–146

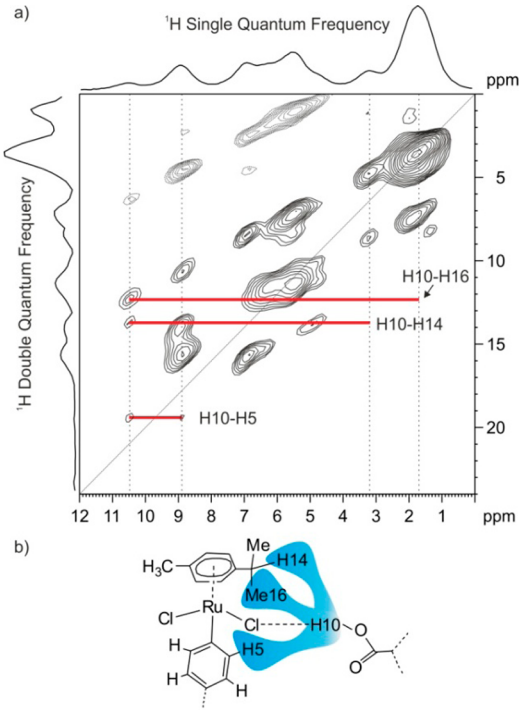

Figure 4. (a) ^{1}H (400.23 MHz) DQ CRAMPS (PMLG5−POSTC7−*w*PMLG5) spectrum of **1γ**, together with skyline projections recorded at 12.5 kHz MAS. Negative contours (artificial peaks) and the F1 = 2F2 diagonal are shown as dashed lines. Solid red horizontal bars indicate specific DQ coherences between OH (H10) and nearby protons. (b) Representation of the crystal structure of **1γ**, showing H10−H16, H10−H14, and H10−H5 proximities.

Table 2. ^{1}H DQ Correlations[a] (in ppm) Involving OH ^{1}H Nuclei (<3.0 Å) in 1α, 1·H$_2$O, 1β, 1γ, and 2[b]

compound	δ_{SQ}	δ_{SQ}	δ_{DQ}	correlation
1α	9.9	5.0	14.9	H10−H11
1·H$_2$O	8.7	1.4	10.1	H10−H16
	8.7	4.7	13.4	H10−Hw
1β	10.1	1.6	11.7	H10−H16 and H15
	10.1	8.5	18.6	H10−H2
1γ[c]	10.5	1.7	12.2	H10−H16
	10.5	3.2	13.7	H10−H14
	10.5	8.9	19.4	H10−H5
2	13.3	0.9	14.3	H10−H16
	13.3	7.8	21.1	H10−H2[d]
	13.3	13.3	26.6	H10−H10

[a]Only intermolecular proximities are reported. [b]See Figures 4 and 5, as well as Figures S4, S5, and S6 in the Supporting Information. [c]In the unit cell, two independent molecules are present. Here, only the molecule with the OH proton involved in the strong O−H···Cl HB is considered. [d]Intramolecular proximity.

independent molecules but does not shed enough light neither on the metrical details of covalent bonding nor on the topology of intermolecular interactions. Indeed, while we clearly observe one short O−H···Cl (O1b···Cl2a) contact and unambiguously exclude the presence of any COOH cyclic dimer, we are unable

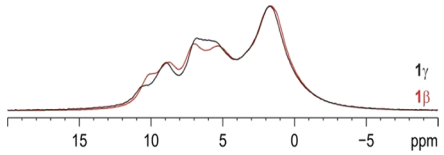

Figure 5. Comparison between ^{1}H (400.23 MHz) MAS spectra of compounds **1β** (red) and **1γ** (black) recorded with a spinning speed of 32 kHz. The technique is quantitative.

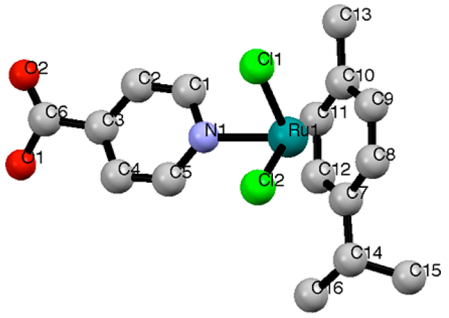

Figure 6. Molecular structure and labeling scheme of **1γ**.

to decide whether the second independent carboxylic group does or does not interact with its closest Cl atom, since the O1a···Cl2b distance is rather elongated and strongly dependent on the details of the antibumping conditions on the nearby atoms. Thus, periodic lattice DFT calculations were performed on the **1γ** XRPD structure in order to increase the accuracy of XRPD results and to ascertain the intermolecular role of this second carboxylic group, and the structure resubmitted for Rietveld refinements. The iteration method, repeated until self-consistency, leads to a final **1γ**-XRPD model.[32] The structure is characterized by one strong O···Cl interaction (O···Cl distance of 3.085 Å and O−H−Cl angle of 166.2°) and one weak O···Cl interaction (O···Cl distance of 3.183 Å and O−H−Cl angle of 156.2°). This agrees with the ^{1}H MAS NMR spectra (see above) and with NMR-GIAO DFT calculations data (in this case GIPAW calculation[33] would be prohibitive). Indeed, both suggested that only half of the OH hydrogen atoms are involved in strong O−H···Cl interactions while the others, attributed to a weaker contact, fall overlapped under the signals of aromatic hydrogen atoms in ortho position, with respect to the pyridine nitrogen atoms (computed chemical shifts: 12.2 and 9.6 ppm for the strong and weak interaction, respectively). Another optimized structure characterized by only one O···Cl contact had higher energy[34] or did not fit XRPD data. The iterative approach adopted herein allowed us to discover, inter alia, that the previously reported **1β** structure had an incorrect conformation of the *p*-cymene *i*-propyl group (see above). We were able to find a better R_{wp} minimum (6.52 vs 6.79) in which the *i*-propyl group has the same conformation found in **1·H$_2$O**. Accordingly, the last sentence of page 4371 of ref 9 must be reconsidered (and Figure 13b modified) given that the molecules in **1·H$_2$O** and **1β** differ only in the carboxyl rotation (see the Supporting Information). The new **1β** XRPD model was then resubmitted to Quantum Espresso, leading to a O···Cl distance of 3.086 Å (OH···Cl distance = 2.106 Å; C−H−Cl angle = 162.6°). This interaction is relatively strong, and fits perfectly with the SSNMR observation of a single strong O−H···Cl HB.

dx.doi.org/10.1021/ic401762z | *Inorg. Chem.* 2014, 53, 139−146

Finally, **1*β*** and **1*γ*** polymorphs have very similar absolute energy per molecule. This observation is also in agreement with the overall picture proposed.

HB Network Analysis. High-resolution ^{1}H 1D (Figure 7, together with the corresponding HB contacts) and 2D DQ CRAMPS (see Figures 3 and 4, as well as Figures S4–S8 in the Supporting Information) SSNMR spectra (**1*α***, **1*β***, **1*γ***, **1·H$_2$O**, and **2**) allowed the HB networks of all polymorphs to be elucidated and confirmed the accuracy of the **1*β*** and **1*γ*** structures solved from powder data. All OH proton chemical shifts with main ^{1}H–^{1}H proximities obtained from the 2D spectra are listed in Table 2.

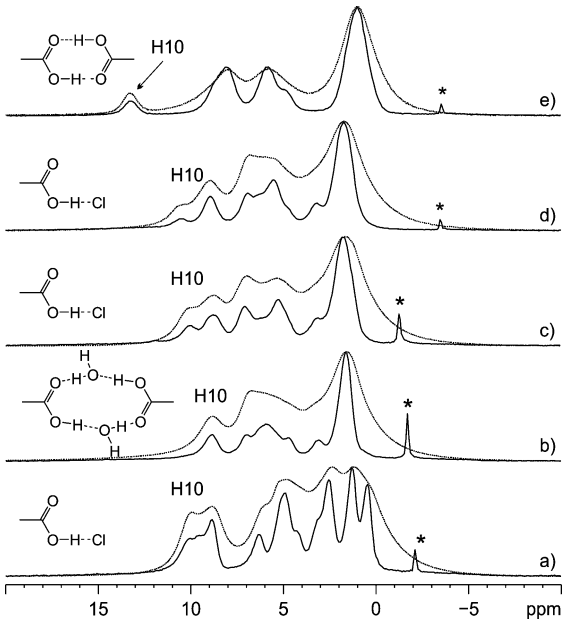

Figure 7. ^{1}H (400.23 MHz) CRAMPS (*w*PMLG5) (black lines) and MAS (gray lines) spectra of compounds **1*α*** (spectrum a), **1·H$_2$O** (spectrum b), **1*β*** (spectrum c), **1*γ*** (spectrum d), and **2** (spectrum e), recorded with spinning speeds of 12.5 kHz (CRAMPS) and 32 kHz (MAS). Assignments of hydrogen-bonded proton signals are also reported with HB network schemes. Asterisks denote carrier frequencies.

While a resolution improvement is observed for all signals by using the *w*PMLG5 method, compared to MAS experiments, we focus our discussion herein on the DQ signals involving hydrogen-bonded protons. X-ray single-crystal structure analysis reveals similar intermolecular hydrogen-bonding arrangements, i.e., the contact O–H···Cl, for the three polymorphs **1*α***, **1*β*** and **1*γ***. This is reflected in similar chemical shift values of the OH resonance at 9.9, 10.1, and 10.5 ppm, respectively. These structures do not show the expected supramolecular cyclic dimerization of the carboxylic functions of INA as confirmed by the lack of diagonal peaks associated to the OH resonance in their ^{1}H DQ CRAMPS spectra (see Figure 4, as well as Figures S4 and S5 in the Supporting Information). This is in agreement with the good HB-acceptor character of the Cl ligands.[35] For **1*β*** DQ signals involving the OH protons are at δ_{DQ} = 10.1 + 1.6 = 11.7 ppm (intermolecular with H15 and H16 - methyl groups of the isopropyl moiety) and δ_{DQ} = 10.1 + 8.5 = 18.6 ppm (intermolecular with H2 - pyridyl aromatic proton of another molecule), see Figure S4 in the Supporting Information. In the ^{1}H 2D DQ CRAMPS spectrum of **1*γ***, we observed proximities between OH and H16 (methyl group of the isopropyl moiety) (δ_{DQ} = 10.5 + 1.7 = 12.2 ppm), OH and H14 (CH group of the isopropyl moiety) (δ_{DQ} = 10.5 + 3.2 = 13.7 ppm) and between H10 and H5 (pyridyl proton) (δ_{DQ} = 10.5 + 8.9 = 19.4 ppm). The ^{1}H–^{1}H proximities observed in the ^{1}H 2D DQ CRAMPS NMR spectra of **1*β*** and **1*γ*** perfectly agree with the structure solved from XRPD and optimized by DFT providing useful parameters for validating the reliability of the structure solved from powder data. In **1*α***, the OH group results quite far from those of other hydrogen atoms, as confirmed by the presence of only one DQ resonance at δ_{DQ} = 9.9 + 5.0 = 14.9 ppm, which is attributed to the H10–H11 (aromatic proton) proximity (see Figure S5 in the Supporting Information). **1·H$_2$O** shows two water molecules bridging two carboxylic functions of two different metallorganic entities, giving rise to a $R^4_4(12)$ supramolecular cyclic dimer.[36] Because of casual overlapping, the location at 4.7 ppm of the proton water signal in the spectrum was possible only through the H10–Hw proximity generating a DQ correlation at δ_{DQ} = 8.7 + 4.7 = 13.4 ppm (see Figure S6 in the Supporting Information). The other correlation refers to the H10–H16 proximity (δ_{DQ} = 8.7 + 1.4 = 10.1 ppm).

As stated above, the **2** analogue presents the supramolecular cyclic dimerization of the COOH group, as highlighted in the ^{1}H DQ CRAMPS spectrum (Figure 3). A similar diagonal peak indicating the COOH dimerization also characterizes the spectrum of the pure ligand A4AB (see Figure S7 and Scheme S1 in the Supporting Information for a sketch of the intermolecular contacts): δ_{DQ} = 13.9 + 13.9 = 27.8 ppm.[37] In contrast, the pure ligand INA presents O–H···N head-to-tail interactions (see Scheme S2 in the Supporting Information),[38] thus its 2D DQ spectrum (see Figure S8 in the Supporting Information) does not shows OH diagonal peaks but DQ signals at δ_{DQ} = 18.1 + 8.5 = 26.6 ppm (OH–H2 and H6 pyridine hydrogen atoms) and δ_{DQ} = 8.2 + 8.2 = 16.4 ppm (H2–H3 and H5–H6 pyridine hydrogen atoms).

Structural Correlation between 1·H$_2$O, 1*γ*, and 1*β*. For comparison, we considered the three structures; **1·H$_2$O** and **1*β*** exhibited a super cell of order 2 with the same space group symmetry ($P2_1/a$) of **1*γ***, and the lattice parameters were similar to those of **1*γ***.

A quick look at Figure 8, where the content of the three (super)cells is reported and the O–H···Cl interactions are highlighted, clearly shows that the entropy-driven water desorption of **1·H$_2$O** (which implies the rupture of 16 O–H···O and 8 O$_w$–H···Cl interactions per supercell) determines a topotactic volume shrinkage (from 3677 Å^3 to 3492 Å^3, which, however, still leaves some residual voids) to **1*γ***, associated with the formation of eight new O–H···Cl interactions per cell. Then, a further volume shrinkage (from 3492 Å^3 to 3389 Å^3) and the reorganization of four, out of eight, O–H···Cl interactions per supercell, leads to **1*β***. Actually, Figure 8A is slightly misleading, since the projection of the structures down the ***c***-axis shades that the **1·H$_2$O** → **1*γ*** phase transition implies not only a doubled cell but also a structural shear along the ***a****-axis at the interface of the carboxylic groups, as highlighted in Figure 9. No additional shear was observed in the following **1*γ*** → **1*β*** transition and, as expected, **1*γ*** is more similar to **1*β*** than to **1·H$_2$O**.

■ CONCLUSION

In this contribution we demonstrate how high-resolution ^{1}H CRAMPS (1D and 2D) SSNMR techniques, XRPD techniques

dx.doi.org/10.1021/ic401762z | *Inorg. Chem.* 2014, 53, 139–146

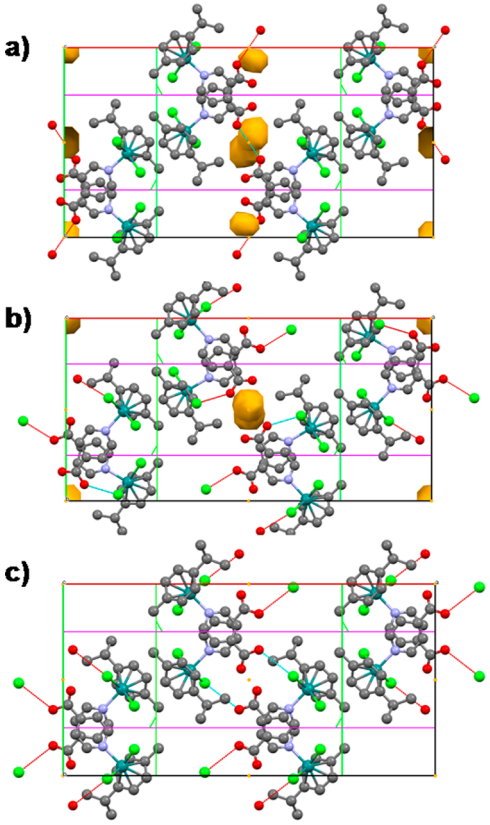

Figure 8. Structure correlation among **1·H$_2$O**, **1*γ***, and **1*β***. All structures have been drawn down their *c*-axis and the O−H···Cl interactions are highlighted. Supercells of (a) **1·H$_2$O**, space group $P2_1/a$, a = 31.57 Å, b = 15.84 Å, c = 7.42 Å, β = 82.25°, V = 3677 Å^3 (water molecules have been omitted for the sake of clarity, but they are located within the volumes highlighted in gold and the carboxylic oxygen atoms mutually interacting through them have been connected by dashed lines); (b) (true) unit cell of **1*γ***, space group $P2_1/a$, a = 30.956 Å, b = 15.358 Å, c = 7.376 Å, β = 95.27°, V = 3492 Å^3 (the golden regions are real "voids" (33 Å^3)); and (c) **1*β***, space group $P2_1/a$, a = 29.32 Å, b = 15.089 Å, c = 7.726 Å, β = 97.03°, V = 3389 Å^3.

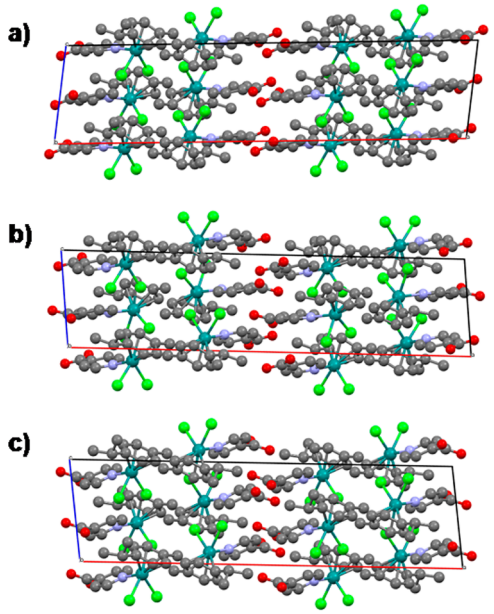

Figure 9. Supercells of (a) **1·H$_2$O**, b) (true) unit cell of **1*γ***, and (c) **1*β***; each drawn down the *b*-axis.

and periodic plane-wave first-principles calculations can be combined for providing reliable structures of organometallic microcrystalline samples not suitable for a single-crystal X-ray analysis.

X-ray powder thermodiffractometry allows us to both follow complex phase transformations and structurally characterize "uncontaminated" intermediates, thus affording substantial information suitable as starting points for SSNMR analysis and DFT plane-wave periodic calculation. On the other hand, SSNMR affords a separate evaluation of the number of crystallographically independent fragments, which is highly useful in the XRPD indexing process. Finally, DFT plane wave periodic calculation together with the ^{1}H−^{1}H proximities, obtained by ^{1}H DQ CRAMPS spectra, provide an efficient method for checking the reliability of the solved structure.

Thanks to this integrated multiple approach, which is intrinsically more accurate than the single methodologies, a complete characterization of the [(*p*-cymene)Ru(*κ*N-INA)Cl$_2$] polymorphic system has been performed. The hydrogen bond networks in all systems have been investigated in term of supramolecular synthons. The phase transformations have been analyzed by thermodiffractometry. Passing from **1·H$_2$O** to **1*γ*** and from **1*β*** to **1*γ***, the sequence of continuous shrinkages and gradual formations of O−H···Cl interactions is coherent with the metastable nature of **1*γ*** at 80 °C. However, we were not expecting to retrieve **1*γ*** upon cooling **1*β*** at room temperature (RT) (under N$_2$ atmosphere), as we later determined.

The structural correlation between **1·H$_2$O**, **1*γ***, and **1*β***, which mainly depends from their space group symmetries, lattice metrics, and rough molecule locations and orientations within the unit cells, has been recognized. Noteworthy, this result greatly improves the level of confidence of our ab initio XRPD structure solution and, possibly, addresses the most probable mechanism of the **1·H$_2$O**, **1*γ***, and **1*β*** polymorphic transformations.

In view of the current interest on the anticancer activity of half-sandwich Ru(II) complexes,[39] the knowledge of the polymorph-dependent stability and hygroscopicity for molecules belonging to this class of compounds (compare the relative affinities of the polymorphs **1*α***, **1*β***, and **1*γ*** toward water) is of paramount importance, since it has a great impact on bioavailability and storage issues.

■ ASSOCIATED CONTENT

Ⓢ Supporting Information

X-ray crystallographic files in CIF format; crystal data for **1*β*** and **1*γ***; additional schemes and figures. This material is available free of charge via the Internet at http://pubs.acs.org.

■ AUTHOR INFORMATION

Corresponding Authors

*E-mail: roberto.gobetto@unito.it (R. Gobetto).
*E-mail: angelo.sironi@unimi.it (A. Sironi).

Author Contributions

The manuscript was written through contributions of all authors. All authors have given approval to the final version of the manuscript.

Notes

The authors declare no competing financial interest.

dx.doi.org/10.1021/ic401762z | *Inorg. Chem.* 2014, 53, 139−146

■ ACKNOWLEDGMENTS

We acknowledge financial support from MIUR (Nos. PRIN2006 and PRIN2007).

■ REFERENCES

(1) (a) Braga, D.; Giaffreda, S. L.; Grepioni, F.; Maini, L.; Polito, M. *Coord. Chem. Rev.* **2006**, *250*, 1267. (b) Lim, G. K.; Fujii, K.; Harris, K. D. M.; Apperley, D. C. *Cryst. Growth Des.* **2011**, *11*, 5192. (c) Long, S.; Parkin, S.; Siegler, M.; Brock, C. P.; Cammers, A.; Li, T. L. *Cryst. Growth Des.* **2008**, *8*, 3137.

(2) (a) Braga, D.; Grepioni, F.; Maini, L.; Prosperi, S.; Gobetto, R.; Chierotti, M. R. *Chem. Commun.* **2010**, *46*, 7715. (b) Lou, B. Y.; Hu, S. L. *J. Chem. Cryst.* **2011**, *41*, 1663. (c) Braga, D.; Dichiarante, E.; Palladino, G.; Grepioni, F.; Chierotti, M. R.; Gobetto, R.; Pellegrino, L. *Cryst. Eng. Commun.* **2010**, *12*, 3534.

(3) Masciocchi, N.; Sironi, A. *Dalton Trans.* **1997**, 4643−4650.

(4) (a) Tobbens, D. M.; Glinneman, J.; Chierotti, M. R.; van de Streek, J.; Sheptyakov, D. *Cryst. Eng. Commun.* **2012**, *14*, 3046. (b) Schmidt, M. U.; Bruning, J.; Glinnemann, J.; Hutzler, M. W.; Morschel, P.; Ivashevskaya, S. N.; van de Streek, J.; Braga, D.; Maini, L.; Chierotti, M. R.; Gobetto, R. *Angew. Chem., Int. Ed.* **2011**, *50*, 7924. (c) Masciocchi, N.; Galli, S.; Alberti, E.; Sironi, A.; Di Nicola, C.; Pettinari, C.; Pandolfo, L. *Inorg. Chem.* **2006**, *45*, 9064.

(5) (a) Bradley, J. P.; Velaga, S. P.; Antzutkin, O. N.; Brown, S. P. *Cryst. Growth Des.* **2011**, *11*, 3463. (b) Chierotti, M. R.; Gobetto, R. *CrystEngComm* **2013**, *15*, 8599.

(6) (a) Lesage, A.; Sakellariou, D.; Hediger, S.; Elena, B.; Charmont, P.; Steuernagel, S.; Emsley, L. *J. Magn. Reson.* **2003**, *163*, 105. (b) Vinogradov, E.; Madhu, P. K.; Vega, S. *Chem. Phys. Lett.* **2002**, *354*, 193. (c) Schnell, I.; Spiess, H. W. *J. Magn. Reson.* **2001**, *151*, 153.

(7) (a) Chierotti, M. R.; Gobetto, R. In *Supramolecular Chemistry: From Molecules to Nanomaterials*; Gale, P. A., Steed, J. W., Eds.; John Wiley & Sons, Ltd.: Chichester, U.K., 2012; pp 331−345. (b) Chierotti, M. R.; Gobetto, R. *Chem. Commun.* **2008**, 1621.

(8) (a) Beko, S. L.; Thoms, S. D.; Bruning, J.; Alig, E.; van de Streek, J.; Lakatos, A.; Glaubitz, C.; Schmidt, M. U. *Z. Kristallogr.* **2010**, *225*, 382. (b) Bradley, J. P.; Pickard, C. J.; Burley, J. C.; Martin, D. R.; Hughes, L. P.; Cosgrove, S. D.; Brown, S. P. *J. Pharm. Sci.* **2012**, *101*, 1821.

(9) Bacchi, A.; Cantoni, G.; Chierotti, M. R.; Girlando, A.; Gobetto, R.; Lapadula, G.; Pelagatti, P.; Sironi, A.; Zecchini, M. *CrystEngComm.* **2011**, *13*, 4365.

(10) (a) Soldatov, D. V. *J. Chem. Crystallogr.* **2006**, *36*, 747−768. (b) Bacchi, A.; Cantoni, G.; Pelagatti, P.; Rizzato, S. *J. Organomet. Chem.* **2012**, *714*, 81−87.

(11) Bacchi, A.; Carcelli, M.; Pelagatti, P. *Crystallogr. Rev.* **2012**, *18*, 253−279.

(12) (a) Braga, D.; Grepioni, F. *Chem. Soc. Rev.* **2000**, *29*, 229−238. (b) Kumalah, S. A.; Holman, K. T. *Inorg. Chem.* **2009**, *48*, 6860−6872.

(13) Bacchi, A.; Cantoni, G.; Granelli, M.; Mazza, S.; Pelagatti, P.; Rispoli, G. *Cryst. Growth Des.* **2011**, *11*, 5039−5047.

(14) van Rossum, B.-J.; de Groot, C. P.; Ladizhansky, V.; Vega, S.; de Groot, H. J. M. *J. Am. Chem. Soc.* **2000**, *122*, 3465.

(15) Bettini, R.; Menabeni, R.; Tozzi, R.; Pranzo, M. B.; Pasquali, I.; Chierotti, M. R.; Gobetto, R.; Pellegrino, L. *J. Pharm. Sci.* **2010**, *99*, 1855.

(16) Vinogradov, E.; Madhu, P. K.; Vega, S. *Chem. Phys. Lett.* **1999**, *314*, 443.

(17) Hohwy, M.; Jakobsen, H. J.; Edén, M.; Levitt, M. H.; Nielsen, N. C. *J. Chem. Phys.* **1998**, *108*, 2686.

(18) Coelho, A. A. *J. Appl. Crystallogr.* **2003**, *36*, 86.

(19) Coelho, A. A. *J. Appl. Crystallogr.* **2000**, *33*, 899.

(20) We wrote a simple program able to build plenty of the individual-atom to individual-atom penalties necessary to drive the conformational search toward reasonable results.

(21) Cheary, R. W.; Coelho, A. A. *J. Appl. Crystallogr.* **1992**, *25*, 109.

(22) *Topas: General Profile and Structure Analysis Software for Powder Diffraction Data*; Bruker AXS: Karlsruhe, Germany, 2001.

(23) Giannozzi, P.; Baroni, S.; Bonini, N.; Calandra, M.; Car, R.; Cavazzoni, C.; Ceresoli, D.; Chiarotti, G. L.; Cococcioni, M.; Dabo, I.; Dal Corso, A.; de Gironcoli, S.; Fabris, S.; Fratesi, G.; Gebauer, R.; Gerstmann, U.; Gougoussis, C.; Kokalj, A.; Lazzeri, M.; Martin-Samos, L.; Marzari, N.; Mauri, F.; Mazzarello, R.; Paolini, S.; Pasquarello, A.; Paulatto, L.; Sbraccia, C.; Scandolo, S.; Sclauzero, G.; Seitsonen, A. P.; Smogunov, A.; Umari, P.; Wentzcovitch, R. M. *J. Phys.: Condens. Matter* **2009**, *21*, 395502.

(24) Vanderbilt, D. *Phys. Rev. B* **1990**, *41*, 7892.

(25) http://www.quantum-espresso.org/?page_id=190.

(26) Perdew, J. P.; Burke, K.; Ernzerhof, M. *Phys. Rev. Lett.* **1996**, *77*, 3865.

(27) Monkhorst, H. J.; Pack, J. D. *Phys. Rev. B* **1976**, *13*, 5188.

(28) Frisch, M. J.; Trucks, G. W.; Schlegel, H. B.; Scuseria, G. E.; Robb, M. A.; Cheeseman, J. R.; Scalmani, G.; Barone, V.; Mennucci, B.; Petersson, G. A.; Nakatsuji, H.; Caricato, M.; Li, X.; Hratchian, H. P.; Izmaylov, A. F.; Bloino, J.; Zheng, G.; Sonnenberg, J. L.; Hada, M.; Ehara, M.; Toyota, K.; Fukuda, R.; Hasegawa, J.; Ishida, M.; Nakajima, T.; Honda, Y.; Kitao, O.; Nakai, H.; Vreven, T.; Montgomery, Jr., J. A.; Peralta, J. E.; Ogliaro, F.; Bearpark, M.; Heyd, J. J.; Brothers, E.; Kudin, K. N.; Staroverov, V. N.; Kobayashi, R.; Normand, J.; Raghavachari, K.; Rendell, A.; Burant, J. C.; Iyengar, S. S.; Tomasi, J.; Cossi, M.; Rega, N.; Millam, J. M.; Klene, M.; Knox, J. E.; Cross, J. B.; Bakken, V.; Adamo, C.; Jaramillo, J.; Gomperts, R.; Stratmann, R. E.; Yazyev, O.; Austin, A. J.; Cammi, R.; Pomelli, C.; Ochterski, J. W.; Martin, R. L.; Morokuma, K.; Zakrzewski, V. G.; Voth, G. A.; Salvador, P.; Dannenberg, J. J.; Dapprich, S.; Daniels, A. D.; Farkas, Ö.; Foresman, J. B.; Ortiz, J. V.; Cioslowski, J.; Fox, D. J. *Gaussian 09, Revision C.01*; Gaussian, Inc., Wallingford, CT, 2009.

(29) Becke, A. D. J. *Chem. Phys.* **1993**, *98*, 5648.

(30) Lee, C.; Yang, W.; Parr, R. G. *Phys. Rev. B: Condens. Matter* **1988**, *37*, 785.

(31) Brown, S. P.; Xia Zhu, X.; Saalwalchter, K.; Spiess, H. W. *J. Am. Chem. Soc.* **2001**, *123*, 4275.

(32) In practice, this was done by finding the best description of the **1*γ***-DFT model with the rigid groups used in the XRPD analysis via an "only penalties" simulated annealing approach and, subsequently, by optimizing the **1*γ***-XRPD model freeing the rigid body translations but imposing that the refined torsional and rotational degrees of freedom, described in the experimental section, were within a range of 2° of those describing **1*γ***-DFT.

(33) Pickard, C. J.; Mauri, F. *Phys. Rev. B* **2001**, *63*, 245101.

(34) Semiquantitatively analysis done by comparing the absolute energy per molecule of the two cells since **1*γ*** contains exactly twice the atoms of **1*β***.

(35) (a) Brammer, L.; Bruton, E. A.; Sherwood, P. *Cryst. Growth Des.* **2001**, *1*, 277−290. (b) Brammer, L. *Dalton Trans.* **2003**, 3145−3157.

(36) Etter, M. C. *Acc. Chem. Res.* **1990**, *23*, 120.

(37) Note that A4AB is known to exist in two polymorphs: *α* and *β*. (a) Athimoolam, S.; Natarajan, S. *Acta Crystallogr., Sect. C: Cryst. Struct. Commun.* **2007**, *C63*, o514−o517. (b) Gracina, S.; Fischer, A. *Acta Crystallogr., Sect. E: Struct. Rep. Online* **2005**, *E61*, o1242−o1244 (note that only the *α* form presents the supramolecular carboxylic group dimerization; thus, in this article, we refer only to this form).

(38) Takusagawa, F.; Shimeda, A. *Acta Crystallogr., Sect. B: Struct. Crystallogr. Cryst. Chem.* **1976**, *32*, 1925.

(39) (a) Liu, H.-K.; Sadler, P. J. *Acc. Chem. Res.* **2011**, *44*, 349−359. (b) Wang, F.; Abtemariam, A.; van der Geer, E. P. L.; Fernández, R.; Melchart, M.; Deeth, R. J.; Aird, R.; Guichard, S.; Fabbiani, F. P. A.; Lozano-Casal, P.; Oswald, I. D. H.; Jodrell, I. D.; Parsons, S.; Sadler, P. J. *Proc. Natl. Acad. Sci. U.S.A.* **2005**, *102*, 18269−18274.